Environmental Science Nano

PAPER

View Article Online
View Journal | View Issue

Cite this: *Environ. Sci.: Nano*, 2018, 5, 1595

Cu-Doped Fe@Fe_2O_3 core–shell nanoparticle shifted oxygen reduction pathway for high-efficiency arsenic removal in smelting wastewater†

Haopeng Feng,[ab] Lin Tang, *[ab] Jing Tang,[ab] Guangming Zeng, *[ab] Haoran Dong,[ab] Yaocheng Deng,[ab] Longlu Wang,[ab] Yani Liu,[ab] Xiaoya Ren[ab] and Yaoyu Zhou[c]

Received 27th March 2018,
Accepted 12th May 2018

DOI: 10.1039/c8en00348c

rsc.li/es-nano

Studies on the removal of As(III) by Fe-based materials have been carried out for decades, but the time-consuming process and low removal capacity are obstacles for large-scale practical applications. Here, a rapid and efficient technique was proposed for the removal of As(III) using Cu-doped Fe@Fe_2O_3 core–shell nanoparticles (CFF) synthesized by a facile two-step reduction method and aging process, which realized a thorough removal of As(III) from smelting wastewater at neutral pH within 30 min. The copper doped in CFF not only provided two extra oxygen reduction pathways to enhance the molecular oxygen activation, but also improved the electron transfer ability and removal efficiency of As(III). The existence of copper contributed to the rapid oxidization and adsorption of As(III), and the removal rate increased nearly 10-times in the aerobic system. Meanwhile, the proposed Cu-doped Fe@Fe_2O_3 core–shell nanoparticles and shifted oxygen reduction pathway could be easily scaled up for other transition metals, such as Ni. Molecular dynamics (MD) simulations based on the large-scale atomic/molecular massively parallel simulator (LAMMPS) were also employed to investigate the formation process of CFF. Furthermore, the removal efficiency of arsenic in smelting wastewater remained to be 90% after 6 times of cycling. Therefore, the distinctive oxidation activities of CFF hold great promise for applications in arsenic removal.

Environmental significance

Arsenic is one of the most toxic environmental pollutants and has aroused widespread concern. Fe-Based materials, especially nZVI, exhibit not only environmental friendliness but also excellent superior chemical stabilities and are widely applied in the water remediation field. We discovered that the presence of copper or nickel in Fe@Fe_2O_3 can significantly improve the removal efficiency of As(III) by shifting the oxygen reduction pathway which will be conducive to oxidize highly toxic and refractory As(III) to lowly toxicity and easily removed As(V). Meanwhile, it also avoids secondary pollution by copper doping due to the unique core–shell structure. The findings provide a new perspective for the preparation of other transition metal doped Fe@Fe_2O_3 materials for the remediation of environmental pollution.

1. Introduction

Recently, large amounts of industrial effluents containing high concentrations of arsenic have been produced in the non-ferrous metal smelting process, especially in the flue gas acid washing recovery section and the smelting section. These kinds of acidic wastewater may cause great harm to the water environment without appropriate treatment.[1] Currently, Fe-based materials have been demonstrated to effectively remove arsenic and refractory organics,[2–7] particularly nanoscale zerovalent iron (nZVI), which could produce reactive oxygen species (ROSs, *i.e.*, H_2O_2, $^{\cdot}O_2^-$, and $^{\cdot}OH$) by molecular oxygen activation to oxidize and adsorb As(III).[8–12] For instance, Ramos's group reported that nZVI can adsorb and

[a] College of Environmental Science and Engineering, Hunan University, Changsha, 410082, China. E-mail: tanglin@hnu.edu.cn, zgming@hnu.edu.cn; Fax: +86 731 88823701; Tel: +86 731 88822778
[b] Key Laboratory of Environmental Biology and Pollution Control, Ministry of Education, Hunan University, Changsha 410082, China
[c] College of Resources and Environment, Hunan Agricultural University, Changsha 410128, China

† Electronic supplementary information (ESI) available: Supporting information includes synthesis, characterization of nanocomposites, fabrication of the E-Fenton cathode, chemical analysis, models for adsorption kinetics, isotherm experiments and energy consumption, and effects of pH and temperature, as well as raw data of XRD, EDS, and MD simulations and data from control experiment testing and consists of 12 additional sections, 19 figures and 8 tables. See DOI: 10.1039/c8en00348c

transform some highly toxic As(III) into insoluble As(V) in the presence of air and iron particles, and subsequently generate As(V)–Fe(III) and As(III)–Fe(III) precipitates.[13] However, the removal of As(III) by Fe-based materials, especially nZVI, is time-consuming (about 2.0–70.5 h) with low removal capacity,[3–5] because the yield of the ROSs relative to the consumed iron (*i.e.*, Δ(oxidants)/Δ(Fe^0)) was poor in the pH range of 2–11.[14]

Generally, the molecular oxygen activation process induced by nZVI takes place as follows. Firstly, Fe^0 reacts with oxygen to produce H_2O_2 by a two-electron molecular oxygen reduction, accompanied with an Fe(II) release (eqn (1)). Subsequently, the released Fe(II) also reacts with oxygen to produce H_2O_2 *via* a sequential single-electron reduction molecular oxygen activation pathway (eqn (2) and (3)). Then, the *in situ* produced H_2O_2 reacts with Fe(II) to produce $^{\bullet}OH$ (eqn (4)). Ai *et al.* reported that iron oxide formed on the surface of nZVI could favor the single-electron molecular oxygen activation.[15] Because Fe(II) released from Fe^0 would be adsorbed on the iron oxide shell, and then promote the single-electron molecular oxygen activation pathway to produce more ROSs.[16] Our group also found that the removal rate and oxidation capacity of As(III) become stronger by enhancing the single-electron molecular oxygen activation pathway with nZVI.[16] This means that appropriate increases in extra pathways of molecular oxygen activation would improve the yield of ROSs and thus enhance the removal efficiency of As(III) by nZVI.

$$O_2 + Fe^0 + 2H^+ \rightarrow Fe^{2+} + H_2O_2 \quad (1)$$

$$O_2 + Fe^{2+} \rightarrow {}^{\bullet}O_2^- + Fe^{3+} \quad (2)$$

$${}^{\bullet}O_2^- + Fe^{2+} + 2H^+ \rightarrow H_2O_2 + Fe^{3+} \quad (3)$$

$$Fe^{2+} + H_2O_2 \rightarrow Fe^{3+} + {}^{\bullet}OH + OH^- \quad (4)$$

Recent studies have found that Fe/Cu bimetallic particles synthesized by the deposition of Cu^0 on the surface of nZVI can improve the removal rates of pollutants owing to the high potential difference (0.78 V) between Fe and Cu.[17,18] Previous studies suggested that Cu^0 coated on the nZVI surface could promote the corrosion of Fe^0 and the generation of [H] in the absence of oxygen.[17,19] Fe/Cu bimetallic particles can retard the oxidation of nZVI and accelerate the reduction rate, and thus the reactivity of the bimetallic particles is higher than that of nZVI. Although Cu^0 possesses a weaker reduction capacity than nZVI, the reduction potentials of Cu^+/Cu (0.552 V) and Cu^{2+}/Cu (0.341 V) are more negative than that of O_2/H_2O_2 (0.695 V), implying that the reduction of oxygen into H_2O_2 by Cu^0 is still thermodynamically feasible. Hence, Cu^0 may also contribute to the activation of oxygen for the generation of ROSs. For instance, Dükkanci showed that Fe/Cu bimetallic particles could be capable of oxidizing the degradation of Rhodamine B with H_2O_2.[20] Similarly, Xia[21] and Danish[22] also synthesized Fe/Cu bimetallic catalysts and found higher catalytic activities and stabilities for the Fenton oxidation of organic pollutants. However, the influences of Cu^0 on the oxygen reduction pathway and molecular oxygen activation in the Fe/Cu bimetallic system are still unclear. Owing to that the rapid superficial oxidation, passivation and leakage of Cu restrict the generation of ROSs and suppress the wide application of Fe/Cu bimetallic particles. In our previous studies, we found that the core–shell structure can synergistically improve the electron transfer capacity of nZVI, and the formation of the shell guaranteed the sustained activity of the system during the drying, storage, shipping and application processes.[16,23] Thereby, it is theoretically foreseeable that the metal oxide layer coated Fe/Cu nanoparticles would improve the molecular oxygen activation efficiency in the application of nZVI, which has never been investigated so far to the best of our knowledge.

In this study, we synthesized nanoscale Cu-doped Fe@Fe_2O_3 core–shell nanoparticles (CFF) with a two-step reduction method and aging process to systematically explore the effect of copper on molecular oxygen activation and oxygen reduction pathways. A series of experiments are designed to reveal the mechanism of the rapid generation of ROSs and the subsequent aerobic oxidation and removal of As(III) by CFF. The properties of the As(III) removal by CFF in smelting wastewater from the metallurgical industry were investigated. Furthermore, we successfully synthesized Ni-doped Fe@Fe_2O_3 core–shell nanoparticles (NFF) and also demonstrated the applicability of shifted oxygen reduction pathways.

2. Materials and methods

2.1. Chemicals and reagents

All the chemicals used in the study, including $NaBH_4$ (96%), $FeSO_4{\cdot}7H_2O$, $CuSO_4{\cdot}5H_2O$, sodium citrate, tetracycline, and *tert*-butyl alcohol (TBA), are of analytical grade unless specified otherwise. The As(III) stock solutions were prepared using $NaAsO_2$ (Mallinckrodt), and all chemical solutions were made from deionized water.

2.2. Synthesis of CFF

CFF was prepared through a two-step reduction method and aging process altered from our previous studies on Fe@Fe_2O_3 fabrication.[16] In brief, 0.752 mol $CuSO_4{\cdot}5H_2O$ was dissolved in 800 ml deionized water containing a 12.8 mmol sodium citrate stabilizer and then purged with N_2 for at least 40 min. Then, 2.1 M $NaBH_4$ was added dropwise into the Cu^{2+} solution until uniform black particles appeared. The synthetic process was carried out by stirring using a revolving propeller under N_2 protection. 30 mL of 0.45 M $FeSO_4{\cdot}7H_2O$ and 16 mL of 2.1 M $NaBH_4$ aqueous solutions were successively added dropwise into the solution without N_2 protection. After that, the nanoparticles were aged in water for 2 h and then washed with deionized water three times. Finally, the nanoparticles were dried in a vacuum freeze dryer under nitrogen. Besides, CFF nanoparticles with different Fe/Cu mass ratios were also prepared (Fe : Cu = 1 : 1, 1 : 2, 3 : 10, 1 : 5, 1 : 10, and 1 : 20 in

mass). The Nanofer 25 nZVI particles were purchased from the NANOIRON® company (Czech Republic, EU).

For comparison, Fe@Fe_2O_3 and Fe/Cu bimetallic catalysts were prepared as described in Text S1 and S2 of the ESI.† Ni-Doped Fe@Fe_2O_3 and Fe/Ni bimetallic catalysts were also synthesized as described in Text S3 and S4 of the ESI.†

The methods for material characterization are provided in the section Text S5 of the ESI.†

2.3. Smelting wastewater characteristics

Acidic smelting wastewater (initial pH 1–2) containing a high concentration of arsenic was sampled from a metallurgical plant situated in Hengnan County, Hunan Province in southern China. The content of metal elements in the acid smelting wastewater was determined using an inductive coupled plasma emission spectrometer (ICP, Baird PS-6, USA), given in Table S1.†

2.4. Bath experiments

During a typical aerobic removal process, 10 mg of CFF was added into 100 ml of a 3.5 mg L^{-1} As(III) aqueous solution with a shaking speed of 190 rpm. The temperature was kept at room temperature during the process, and the initial pH was adjusted to 7.0 ± 0.2 using 1 M HCl and NaOH solutions. Aliquots of the aqueous solution were withdrawn at intervals and then filtered through 0.45 μm filter membranes for further analysis. For comparison, anoxic removal of As(III) was performed by bubbling nitrogen gas in sealed bottles. After the reaction, the mixture was centrifuged to separate the CFF. The obtained CFF dried using a vacuum freeze dryer was used for further characterization. Methods for chemical analysis are provided in the ESI† sections Text S6 and S7. All experimental data were calculated using the average of three repeated experiments, and the standard deviations were represented by error bars in following plots.

As for the stability test of CFF in practical applications, 80 mg of CFF was added into 100 ml of smelting wastewater, and magnetically separated from the effluent after the reaction for direct reuse in the next batch of wastewater. Before use, the smelting wastewater needs to be diluted with the pH adjusted using the 1 M NaOH solution to be consistent with the simulated wastewater experiment.

3. Results and discussion

3.1. Basic properties of the materials

The prepared CFF composites characterized by scanning electron microscopy (SEM) and transmission electron microscopy (TEM) are composed of abundant nanoparticles with dozens of nanometers in diameter (Fig. 1a and S1†). The TEM image of the CFF analysis further confirmed the

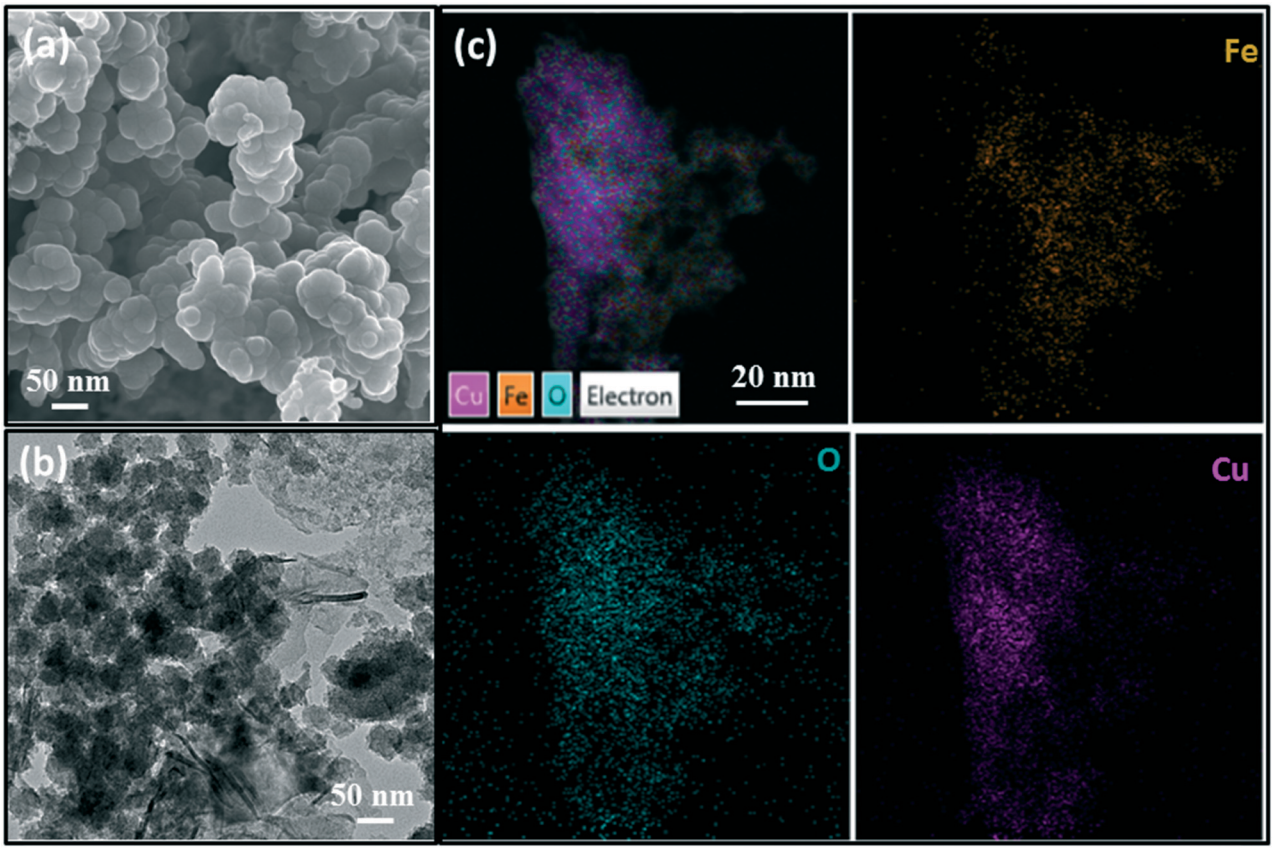

Fig. 1 SEM image (a), and TEM image (b) of CFF; (c) EDS elemental mappings for Cu, Fe, O, and the combined result.

existence of the core–shell structure by contrast of chromatic aberration, and EDS mapping clearly displayed the Fe/Cu nanoparticle core surrounded by a layer of the copper and iron oxide shell (Fig. 1b and c). It can be clearly observed that the O elements are distributed on the surface of the Fe/Cu nanoparticle. In the XRD analysis results (Fig. S2†), an obvious diffraction peak at a 2θ value of 44.6°, which is consistent with the standard pattern of Fe^0 (JCPDS, file No. 65-4899), is observed both in CFF and nZVI. The Fe^0 peak intensity of CFF is weaker than that of nZVI due to the gradual oxidization of Fe^0 with the increase of aging time, consistent with our previous studies.[16] The different peaks at 2θ values of 43.5°, 38.7°, 36.5° and 35.7° related to the standard patterns of Cu, CuO, Cu_2O and Fe_2O_3 were also found in CFF, respectively. According to these results, we can assume that the material was structured with the Fe/Cu nanoparticle surrounded by a layer of the metal oxide shell.

To further distinguish the specificity between the CFF and the common Fe/Cu bimetallic material, we prepared CFF and Fe/Cu bimetallic catalysts with different Cu contents (Cu : Fe = 1 : 1, 1 : 2, 3 : 10, 1 : 5, 1 : 10, and 1 : 20 in mass), and their reactive activity was evaluated by the aerobic removal of As(III) at room temperature. As shown in Fig. 2a and b, the removal capacity of CFF is superior to that of the Fe/Cu bimetallic catalysts. In particular, for CFF with a Cu content of 20% (1 : 5), about 42.0% of As(III) was removed over the Fe/Cu bimetallic catalysts in 30 min, and the CFF showed a higher efficiency of 97.8%. All the kinetic processes were fitted with the pseudo-second order kinetic model (Fig. S3†). The removal rate constant (k_{As}) of CFF is nearly 10 times as much as that of the Fe/Cu bimetallic catalysts when the amount of copper is 20% (Table S2†). These results further demonstrated that CFF possessed the unique core–shell structure that is distinguished from common Fe/Cu bimetallic materials. Furthermore, the removal capacity and rate of As(III) by CFF and the Fe/Cu bimetallic catalysts were initially increased with increasing copper content, but declined when exceeding the optimum content (20%). These results suggest that adding a suitable amount of Cu into nZVI could improve the aerobic removal capacity and rate of As(III). As for the specific reasons, we will have a detailed explanation at the back.

Generally, nZVI can spontaneously react with molecular oxygen to generate ferrous and ferric in the aqueous phase, along with iron oxides and hydroxides produced under aerobic conditions.[8,16,24–26] As(III) may be trapped by the matrix of the growing corrosion products and then be removed from the aqueous solution by precipitation and co-precipitation.[27,28] Additionally, Cu is often used as a catalyst to facilitate the corrosion of Fe^0 owing to the high potential difference between iron and copper, which contribute to the production of H_2O_2 that would trigger a Fenton-like reaction.[29–31] Thus, a certain amount of Cu can improve the removal capacity and rate of As(III) with nZVI, which is similar to our experimental phenomenon. More importantly, it is interesting to note that the removal rate of As(III) by CFF is not only higher than that of the Fe/Cu bimetallic catalysts,

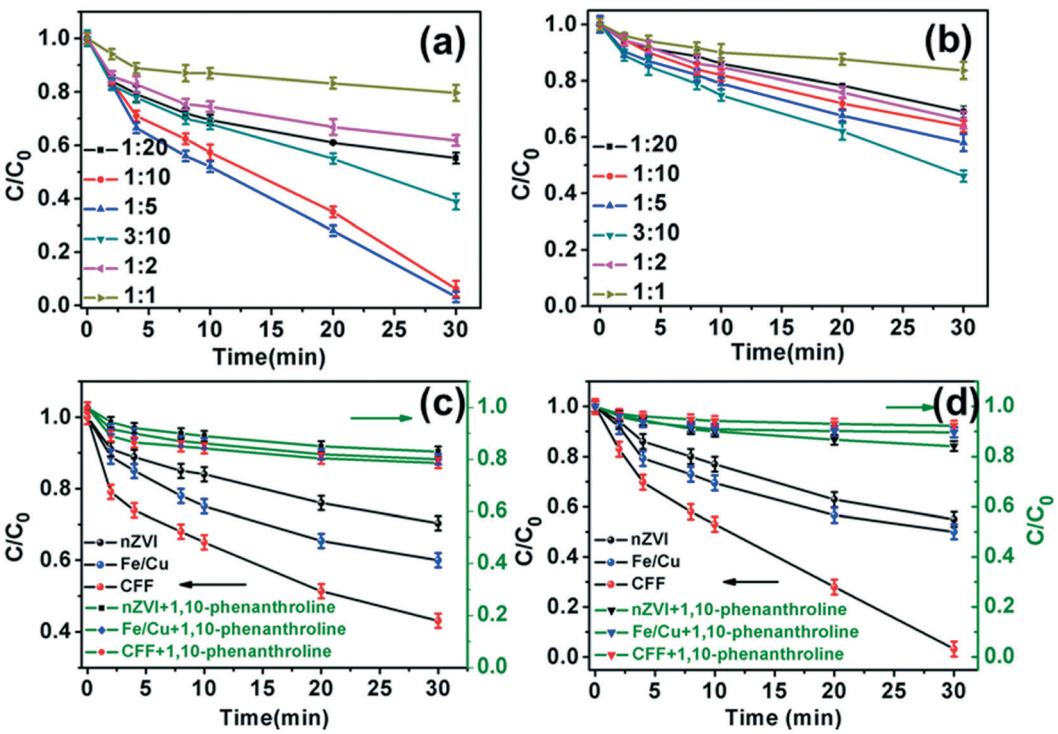

Fig. 2 The temporal concentration change of As(III) as a function of reaction time during the aerobic removal of As(III) over CFF (a) and Fe/Cu bimetallic catalysts (b) with different Fe/Cu mass ratios; efficiency of anoxic As(III) removal (c) and aerobic removal (d) over nZVI, Fe/Cu bimetallic, and CFF catalysts with and without 1,10-phenanthroline. The initial CFF was 100 mg L^{-1}, As(III) was 3.5 mg L^{-1}, and the pH values were 7.0 ± 0.2.

but also superior to most other Fe-based materials (Table 1), which provides the possibility for rapid removal of arsenic from wastewater by Fe-based materials in practical applications.

3.2. Mechanisms for enhanced removal capacity of As(III)

To find out the internal mechanism about why As(III) can be rapidly removed by CFF, we carried out a series of verification tests in which the Cu content in both CFF and Fe/Cu bimetallic catalysts was 20% unless otherwise specified.

To confirm the indispensable role of Fe(II) on the removal of As(III), we compared the removal efficiency of As(III) using different materials in oxygen free water firstly with the 1,10-phenanthroline method. In the absence of oxygen conditions, the apparent removal efficiencies of As(III) were 57%, 40%, and 30% for CFF, Fe/Cu, and nZVI, respectively. The As(III) removal abilities were considerably decreased when 1,10-phenanthroline was added to complex the soluble Fe(II) (Fig. 2c), suggesting that the removal performance of As(III) was strongly dependent on the existence of Fe(II) in anoxic environments rather than the adsorption capacity of the material itself. The surface area could also affect the removal efficiency of adsorbents, so the BET surface areas of the CFF and the common Fe/Cu bimetallic material with the Cu content of 20% (1 : 5) were measured, and their removal rate constants were compared (Table S2†). The results showed that there is little change in the specific surface area of the two samples, suggesting that the different reactivities of CFF and the Fe/Cu bimetallic material are not attributed to the surface area, but to the unique core–shell structure. Our preliminary experiments suggested that the As(III) removal is mainly attributed to the corrosion products formed by Fe(II), since they will react with As(III) to generate an inner-sphere complex, and the generation of iron hydroxide can also adsorb As(III) through co-precipitation.[16] As observed in Fig. S4,† the results revealed that CFF possessed a higher initial Fe(II) concentration and a faster Fe(II) release rate than its counterparts in the presence of 1,10-phenanthroline under anoxic conditions, because the presence of a metal oxide shell, such as Fe_2O_3, could absorb more Fe(II) on its surface, and the existence of Cu^0 might facilitate the corrosion of metallic iron. Furthermore, Fe_2O_3 is also a highly efficient adsorbent for arsenic removal by the electrostatic attraction force and the covalent bonding force.[32] The apparent pseudo-second anoxic As(III) removal rate constants of the CFF, Fe/Cu, and nZVI catalysts with 1,10-phenanthroline were 0.0037, 0.0045, and 0.0039 min^{-1}, respectively, much lower than those without 1,10-phenanthroline (Fig. S4b and S5a†). The inhibitory efficiency (η) of 1,10-phenanthroline during the anoxic As(III) removal was thus calculated using eqn (5).

$$\eta = \left[\frac{k_0 - k_t}{k_0}\right] \times 1 \quad (5)$$

where k_t and k_0 are the apparent As(III) removal rate constants in the presence and absence of 1,10-phenanthroline, respectively. The inhibitory efficiencies of CFF, Cu/Fe, and nZVI were found to be 80.2%, 70.3%, and 57.2%, respectively (Fig. S5a†). This confirmed that the existence of copper, especially the copper serving as the core surrounded by a layer of metal oxide, is beneficial to promote the corrosion of metallic iron and to enhance the removal efficiency of As(III). Maybe it's because the activity of Cu^0 was preserved to the greatest extent.

The same phenomenon also occurs in aerobic aqueous solution. However, compared to the removal efficiency of 57.0% under anoxic conditions, 97.8% of As(III) was removed within 30 min in the presence of oxygen (Fig. 2d). The contribution of Fe(II) achieved an 89% removal of As(III), in contrast, only 36% was obtained under anoxic conditions (Table S3†). Meanwhile, the removal rate of As(III) by CFF is 0.117 min^{-1} in the presence of oxygen, nearly 5 times as much as that under anoxic conditions, implying that molecular oxygen could also improve the removal capacity of As(III) over CFF (Fig. S5b†). A similar phenomenon was also found in nZVI and Fe/Cu bimetallic catalysts (Table S3†). The effect of the electron transfer property on the aerobic As(III) removal performance of CFF, Fe@Fe_2O_3, Fe/Cu, and nZVI was subsequently checked by measuring the free corrosion potentials of these materials using Tafel polarization diagrams. The free corrosion potentials of CFF and its counterparts are in the range of −0.35 to −0.70 V, and their negative potentials follow a trend of CFF > Fe/Cu > Fe@Fe_2O_3 > nZVI (Fig. 3a). It is

Table 1 Comparison of As(III) removal by various Fe-based materials reported in the literature compared with CFF

Materials	pH	As(III) conic (mg L^{-1})	Removal time (min)	Removal rate (%)	Adsorbent conic (mg L^{-1})	Ref.
Bare nZVI	7.0	1.0	720	100	1000	4
Activated carbon supported nZVI	6.5	2.0	4230	100	1000	51
Fe@Fe_2O_3 nanobunches	7.0 ± 0.2	2.3	360	92	50	52
Redox polymer-based Fe(III) oxide nanocomposite	7.0	1.0	1302	100	500	5
Fe/Al bimetallic particles	7.0	10.0	120	100	3000	3
Fe/Cu binary oxide	7 ± 0.1	10.0	360	100	200	53
Fe/Al hydroxide coated onto macroporous supports	7.0	1.0	450	95	700–800	54
Hollow Fe–Ce alkoxides	6.0	10.0	240	92.7	200	2
CFF	7.0 ± 0.2	3.5	30	97.8	100	This work

Conic: concentration.

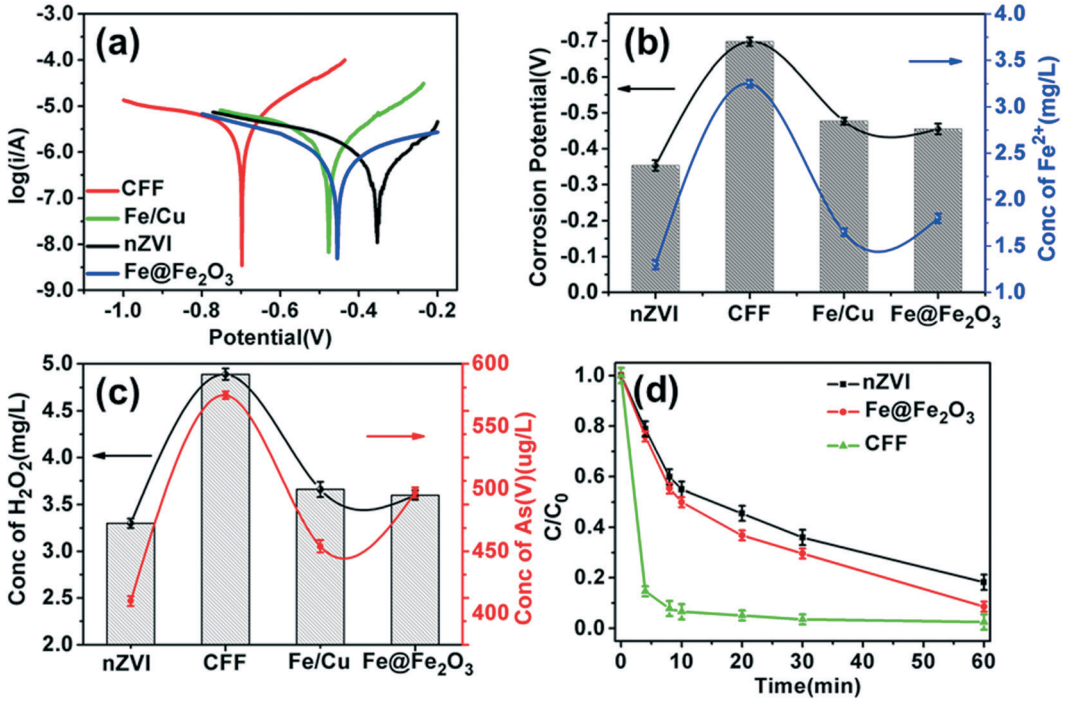

Fig. 3 (a) Tafel scans under aerobic conditions. (b) Free corrosion potentials of CFF, Fe/Cu bimetallic, nZVI, and Fe@Fe_2O_3 catalysts along with the maximum Fe(II) released concentration. (c) The maximum H_2O_2 and As(V) generated concentrations. (d) The temporal concentration of H_2O_2 as a function of time in the nZVI/air, Fe@Fe_2O_3/air, and CFF/air systems, the initial concentration of H_2O_2 was 1.68 mM.

common knowledge that the electrode with a more negative free corrosion potential value would tend to lose electrons easier and faster.[33,34] Therefore, the electron transfer rates of CFF and its counterparts in the aerobic As(III) aqueous solution also followed the above trend, consistent with that of the normalized apparent Fe(II) released concentrations of these materials (Fig. 3b and S6†). This means that CFF has a higher capacity to activate molecular oxygen than its counterparts, since a less reactive species Fe(IV) can't oxidize As(III) to As(V) as an active Fenton intermediate at neutral pH values.[35] In our previous study, it was found that oxidation and adsorption are both present during the As(III) removal process by Fe@Fe_2O_3 under aerobic conditions. That is because Fe@Fe_2O_3 can activate molecular oxygen by both a two-electron transfer route from the Fe^0 core to oxygen to generate H_2O_2, followed by the production of $^{\cdot}OH$ with Fe(II), and a single-electron transfer route from the surface bound Fe(II) to oxygen to generate $^{\cdot}O_2^-$.[9] The produced $^{\cdot}OH$ and $^{\cdot}O_2^-$ with strong oxidative abilities could oxidize As(III) to easily removed As(V), which undoubtedly accelerates the removal of As(III). Meanwhile, Ai's group found that nanoscale zero-valent copper could reduce O_2 to H_2O_2 (eqn (6) and (7)), which would react with Cu(I) and Cu(II) to produce $^{\cdot}OH$ and $^{\cdot}O_2^-$, respectively (eqn (8) and (9)).[36] On the basis of the above discussion and results, we suspect that the existence of Cu^0 could enhance the ability of CFF to react with molecular oxygen to produce reactive oxygen species, thus leading to the amazing capability of CFF for As(III) removal.

$$2Cu + O_2 + 2H_2O \rightarrow 2Cu^+ + H_2O_2 + 2OH^- \quad (6)$$

$$Cu + O_2 + 2H_2O \rightarrow Cu^{2+} + H_2O_2 + 2OH^- \quad (7)$$

$$Cu^+ + H^+ + H_2O_2 \rightarrow Cu^{2+} + {}^{\cdot}OH + H_2O \quad (8)$$

$$Cu^{2+} + H_2O_2 \rightarrow Cu^+ + {}^{\cdot}O_2^- + 2H^+ \quad (9)$$

To confirm this opinion, the production of H_2O_2 with different materials was measured. And the results suggested that CFF exhibited higher H_2O_2 production than Fe/Cu, Fe@Fe_2O_2, and nZVI. The maximum yields of H_2O_2 of CFF and its counterparts followed the order of CFF > Fe/Cu > Fe@Fe_2O_2 > nZVI (Fig. 3c). Obviously, this order was partially in agreement with that of their free corrosion potentials in the aerobic aqueous solution. The concentration of dissolved oxygen in the aqueous solution during the As(III) removal process by CFF was also measured (Fig. S7†). There is no vast turnaround in concentration. This is because the surging solution will bring a lot of air into the water, producing a large number of different sizes of bubbles. Under the hydrostatic pressure of the water body, the bubbles will release a lot of air into the water to become dissolved oxygen due to the internal and external pressure difference.[37,38] Thus, the sufficient dissolved oxygen almost guaranteed the production of H_2O_2. It was also found that more As(III) were oxidized in the aerobic system using CFF compared to those using its counterparts after 20 min of reaction (Fig. 3c). As the amount of accumulated H_2O_2 was heavily dependent on both its formation (eqn (1), (3), (6) and (7)) and decomposition (eqn (4), (8) and (9)) under aerobic conditions, the decomposition rates of H_2O_2 ($(H_2O_2)_{initial}$ =

1.68 mM) over CFF, nZVI, and Fe@Fe_2O_3 under an aerobic atmosphere were also studied (Fig. 3d), and it was found that the decomposition rate of H_2O_2 in the aerobic CFF system was higher than the others, suggesting that the presence of copper could accelerate the decomposition of H_2O_2 on CFF. According to the higher production and faster decomposition of H_2O_2 in the aerobic CFF system, it could be concluded that Cu^0 could greatly promote the formation of H_2O_2 by CFF *via* molecular oxygen activation. In order to further verify the contribution of copper, a number of control experiments were subsequently conducted in an aerobic nZVI system after the addition of different concentrations of Cu(II). As shown in Fig. 4a, the aerobic As(III) removal capacity increased with the increasing concentration of Cu(II), and then decreased after reaching the optimum concentration. This phenomenon is consistent with the previous conclusions. The existence of copper can promote the corrosion of metallic iron and produce more iron oxide and hydroxides that are beneficial to the adsorption and co-precipitation of arsenic. To eliminate the effect of metallic iron on the activation of molecular oxygen, we also employed 1,10-phenanthroline to complex both the *in situ* formed Fe(II) released from CFF into aqueous solution and the surface bound Fe(II) on the CFF.[39] As illustrated in Fig. 4b, the arsenic removal efficiencies of CFF were almost completely suppressed after adding 1,10-phenanthroline, while the process of oxidization of As(III) to As(V) remained. It means that Cu^0 produced the ROSs by the sequential single-electron transfer route (eqn (6) and (8)) and the two-electron transfer route (eqn (7) and (9)). Meanwhile, Cu(I) and Cu(II) could be released from Cu^0 (eqn (7) and (8)), as confirmed by the Cu 2p XPS spectra of the freshly prepared CFF and the used CFF (Fig. 5a); the content of Cu^0 decreased from 44.4% to 31.6%. In contrast, the amount of Cu(I) and Cu(II) increased from 26.0% and 29.6% to 33.9% and 34.5%, respectively (Table S4†). It is known that $^{\cdot}OH$ can be generated through the catalytic decomposition of H_2O_2 by Cu(I) *via* the Fenton-like reaction (eqn (8)).[40,41] The appearance of $^{\cdot}O_2^-$ perhaps catalyzed the decomposition of H_2O_2 by Cu(II) (eqn (9))[42,43] because Cu^0 of less reducibility could not reduce O_2 to $^{\cdot}O_2^-$ $\left(E^0_{O_2/^{\cdot}O_2^-} = -0.33\ V\right)$.

Subsequently, the active species trapping experiments were investigated to check the effect of radicals in the aerobic CFF system by using TBA as the $^{\cdot}OH$ scavenger and *p*-benzoquinone as the $^{\cdot}O_2^-$ scavenger (Fig. S8†).[44,45] Our previous experiments suggested that negligible As(III) could be oxidized to As(V) by H_2O_2, thus the comparison of the inhibitory effects on the aerobic CFF system for the pollutant removal could reflect whether radials were generated.[16] Obviously, the pollutant removal efficiencies of the aerobic CFF systems were both decreased by 10% after the addition of TBA or *p*-benzoquinone. Meanwhile, the results suggested that the CFF/air system would rapidly oxidize As(III) to As(V) without adding TBA or *p*-benzoquinone to the aqueous solution, while the oxidation of As(III) no longer happened when TBA or *p*-benzoquinone was added (Fig. S9a†). As shown in Fig. S9b,† the As(III) removal rate significantly dropped by nearly half with the addition of TBA or *p*-benzoquinone, suggesting that both $^{\cdot}O_2^-$ and $^{\cdot}OH$ play important roles during As(III) oxidation. Surprisingly, with the addition of either TBA or *p*-benzoquinone, the As(III) removal rate of CFF is higher than that of the Fe/Cu bimetallic catalyst (Table S5†). This phenomenon is probably traceable in the metal oxide layer, because the Cu^0 and Fe^0 were protected from oxidation or passivation in the storage and transportation process, thus maintaining higher activity compared to the common Fe/Cu bimetallic catalyst. Hence, the presence of Cu^0 could promote the CFF to activate molecular oxygen for the production of H_2O_2, $^{\cdot}OH$, and $^{\cdot}O_2^-$ to further oxidize As(III). Meanwhile, the generated Cu(II) would further react with Fe^0 to promote the corrosion of metallic iron, and then regenerate Cu^0, and thus forming a benign cycle of arsenic removal. The study also further explained the reason why the CFF has higher Fe(II) releasing capacity and stronger activated molecular oxygen ability than nZVI, Fe@Fe_2O_3 and Fe/Cu bimetallic catalysts. The obviously macroscopic difference of the As(III) in aqueous solution removed by CFF with or without TBA and

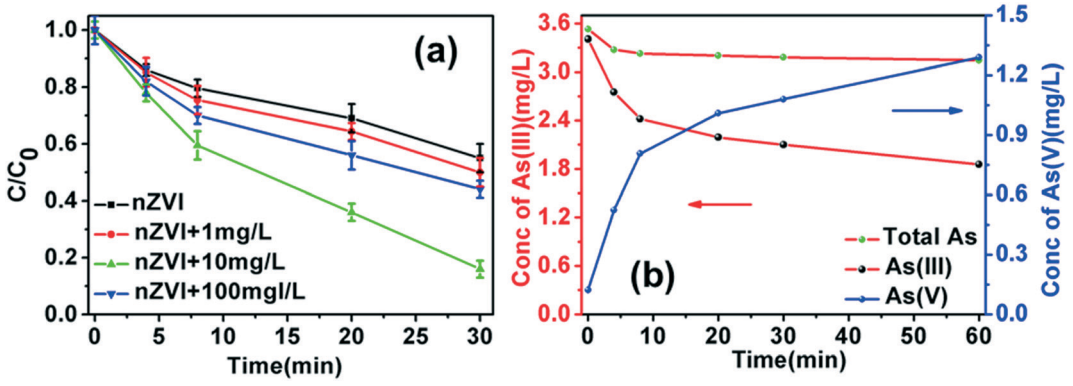

Fig. 4 (a) Effect of initial concentration of copper ion on the aerobic removal of As(III) by nZVI. (b) Changes of the concentrations of As(III), As(V) and total arsenic by the CFF/air system in the presence of 1,10-phenanthroline.

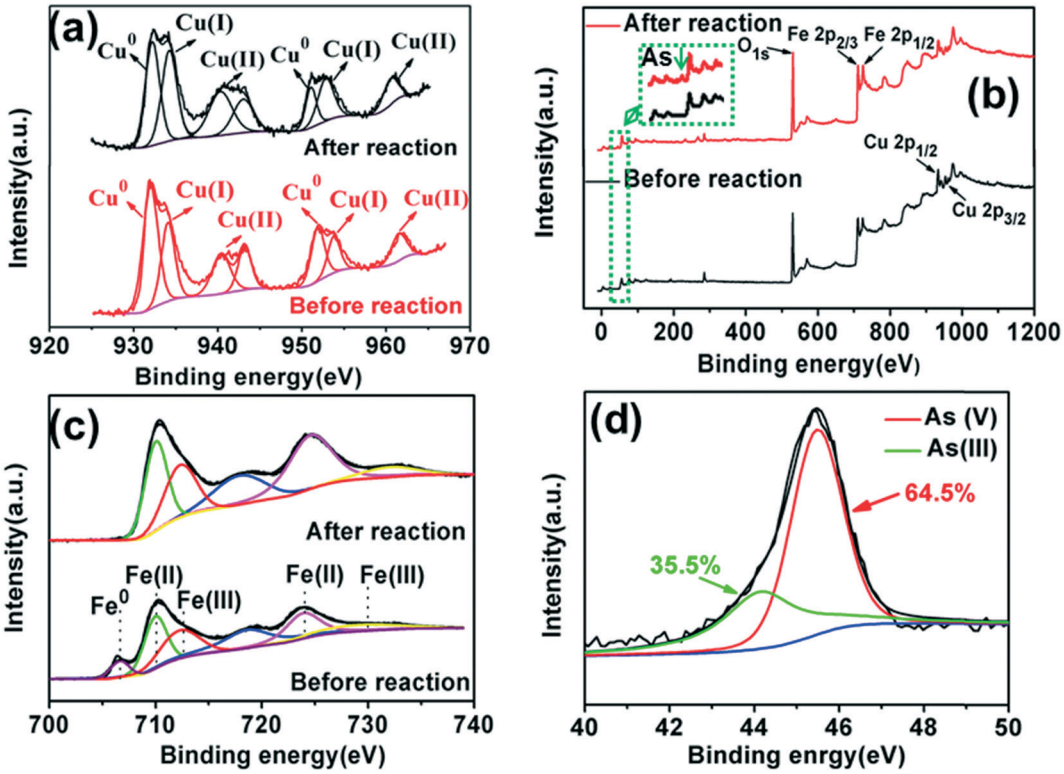

Fig. 5 (a) XPS response of detailed survey for the region of Fe 2p for CFF before and after reaction with As(III) under aerobic conditions. (b) Cu 2p spectra before reaction and after reaction with As(III). (c) Full survey spectra for CFF before and after reaction with As(III) under aerobic conditions. (d) As 3d XPS spectra of CFF after reaction with As(III).

p-benzoquinone (Fig. S9c and d†) further proved that radicals play a vital role in the removal process of As(III). They can not only oxidize As(III) to As(V), but also improve the generation of iron oxide/hydroxide.

The changes in the composition of the CFF surface before and after reaction were further analyzed using XPS techniques. The XPS spectra demonstrated that the prepared CFF contains the elements O, Cu and Fe (Fig. 5b). After CFF reacted with As(III), a new weak characteristic peak of arsenic was observed at 45.5 eV in the full survey of As(III), indicating that the arsenic was adsorbed on the surface of the treated CFF. Furthermore, the results demonstrated that arsenic was uniformly dispersed on the surface of CFF after reaction by EDS mapping analysis (Fig. S10†). Besides, Cu appeared on the surface of the metal oxide after reaction, confirming that copper ions were released from Cu^0 and then reacted with Fe^0. Finally, the surface of CFF was covered by the formed copper oxide. Various valence states of iron, Fe^0, Fe^{II}, and Fe^{III}, coexisted in CFF (Fig. 5c). In the aging process, the iron oxide shell would be generated through the reaction of Fe^0 with dissolved oxygen and water, and then release Fe(II) to the aqueous solution. The oxide shell would adsorb the leached Fe(II), resulting in the higher initial content of Fe(II) of CFF than those of its counterparts. Apparently, the peak of Fe^0 disappeared and the peak of Cu^0 decreased after reaction, implying that they were both involved in the removal process of As(III). Therefore, the XPS analyses also revealed the reason why CFF can rapidly and effectively remove As(III). XPS was also applied to determine arsenic oxidation states on iron (hydr)oxide, and the peak positions were identified by comparison to As3d binding energies reported in the literature.[13] The peaks of As(V) and As(III) were clearly observed on reacted CFF under aerobic conditions (Fig. 5d). Compared to our previous work, although more aqueous As(III) were oxidized to As(V), there was still a small fraction of As(III) that was not completely oxidized. Due to the rapid oxidation of Fe(II) and the generation of Fe (oxyhydr)oxides at neutral pH, some of the As(III) could be removed before oxidation. The same phenomenon can be observed in a previous report.[46] Meanwhile, nearly 64.5% As(III) was oxidized to As(V) on the surface of iron (hydr)oxide, higher than our previous data (35%)[16] under aerobic conditions, further supporting that the Cu doping enhanced the ability of CFF to activate molecular oxygen and produce more ROSs, which will be conductive to oxidize highly toxic and refractory As(V).

Based on the above discussion, a possible mechanism was proposed to account for the rapid removal of As(III) with CFF under aerobic conditions. In the absence of Cu^0, $Fe@Fe_2O_3$ can activate molecular oxygen only by a two-electron transfer route from Fe^0 to oxygen to produce H_2O_2 (eqn (1)) and by a single-electron transfer reaction from the surface bound Fe(II) to oxygen to generate $^{\cdot}O_2^-$ (eqn (2)). Interestingly, two extra

electron transfer paths of molecular oxygen activation were added to CFF when copper was doped, accompanied with the enhanced electron transfer ability that leads to rapid purification of arsenic containing wastewater. That's because Cu^0 could reduce molecular oxygen *via* single-electron and two-electron reduction pathways to produce H_2O_2.[47] Meanwhile, MD simulations based on LAMMPS were employed to investigate the formation process of CFF. The result revealed an interesting phenomenon that copper has a tendency to move toward the core (Fig. S11†). It means that the activity of Cu^0 can be preserved to the greatest extent. As Cu(I) and Cu(II) leach into the aqueous solution during the process, the generated H_2O_2 would then react with both dissolved Cu(II), Cu(I) and Fe(II) to produce $^{\cdot}O_2^-$ and $^{\cdot}OH$ for the oxidative removal of As(III). The *in situ* released copper ions could be reduced by Fe^0 and then deposited on the surface of CFF. With increasing the content of copper, more copper reduced by Fe^0 were deposited on the surface of CFF, which undoubtedly decreased the electron transport rate and suppressed the corrosion of CFF, resulting in the decrease of the As(III) removal capacity. In order to avoid secondary pollution by copper doping, the concentration of leaked copper ions during the removal of As(III) was also measured. On the one hand, copper ions can be reduced by Fe^0 to re-cover the surface of CFF, but on the other, they can also be oxidized by oxygen and ROSs to generate a precipitate. Furthermore, the produced iron oxide and hydroxide can also remove copper ions by adsorption and co-precipitation. Therefore, the results revealed that no secondary pollution occurred (Table S6†). We also successfully prepared NFF with nickel doped Fe@Fe_2O_3 by adopting the same method to further test the applicability of our fabrication technique and verify our conclusion. Interestingly, we observed the same phenomenon that the existence of nickel could promote the removal capacity of As(III) compared to common Fe/Ni bimetallic catalysts (Fig. S12†).

3.3. Effects of pH and temperature

The influence of pH on As(III) removal by CFF is elucidated in Fig. 6a. The removal of As(III) was highly pH dependent, and the amount of As(III) uptake increased with increasing pH from 3.0 to 7.0, and then declined when pH > 7.0. It is well known that As(III) could be captured by protonated hydroxyl groups of iron oxides by inner-sphere complex formation.[48,49] The amount of protonated hydroxyl groups and ROSs decreased at higher pH values, thereby leading to the decrease of As(III) removal. Additionally, we found that all the pH values will eventually stabilize around 7 except the solution with an initial pH of 11, and CFF exhibited a commendable removal efficiency of As(III) at a broad pH (3.0–9.0), suggesting that CFF possessed a potential possibility for the treatment of As(III) in most surface water and groundwater under natural conditions (Fig. 6b). This is because the existence of a metal oxide shell, Fe^0 and Cu^0, could consume H^+

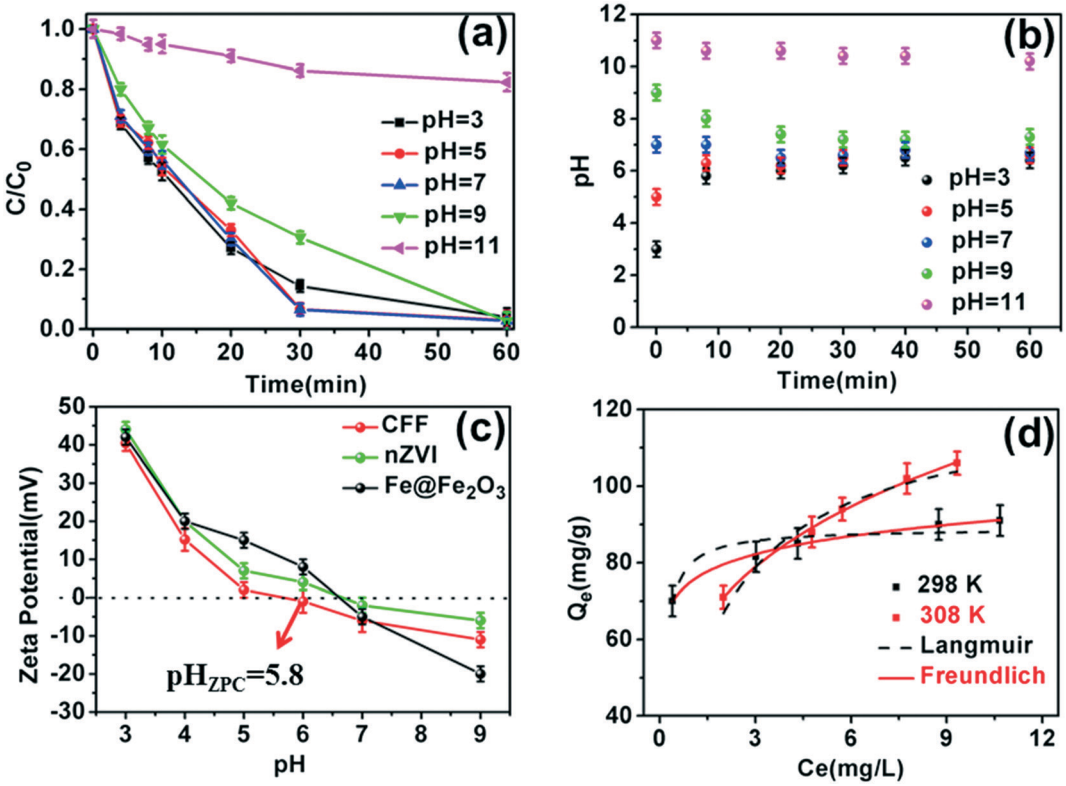

Fig. 6 (a) Effect of pH on As(III) removal by CFF. (b) Time profiles of the pH values of the As(III) solution during its removal in the CFF/air system. (c) Zeta potentials of CFF, nZVI and Fe@Fe_2O_3 in aqueous solutions at various pH values. (d) Langmuir and Freundlich isotherm models for As(III) adsorption at different temperatures onto CFF. C[As(III) initial] = 3.7–6.7 mg L^{-1}, pH 7.0 ± 0.2.

in acidic systems, and the iron ions adsorbed on the surface of CFF could consume OH^- in alkaline systems. This leads to wider pH adaptability for CFF. The surface charges of the CFF, nZVI and Fe@Fe_2O_3 at different pH values are elucidated in Fig. 6c. The results indicate that the CFF has a lower pH_{ZPC}. It means that CFF has higher removal efficiency for As(III) than its counterparts under neutral conditions. The solid surface is negatively charged at pH values above the zero point charge (pH_{ZPC}) and positively charged at pH values below pH_{ZPC}, which will enhance electrostatic repulsion and attraction, respectively, with anionic arsenic species and increase adsorption capacity.

As suggested in Fig. 6d, the removal capacity increased as the temperature was raised from 298 K to 308 K, which was possibly ascribed to the enhanced mobility of ions along with the increase of the reaction temperature.[50] Meanwhile, the As(III) removal process fits better with the Freundlich model with a correlation coefficient R^2 value of 99%, indicating that As(III) removal is not simply a monolayer coverage but also involves an oxidation reaction (Text S8†). The pseudo-second order adsorption kinetics model aligns well with these experimental data obtained in both low and high initial As(III) concentrations under the aerobic conditions, suggesting that chemisorption governs the removal process (Fig. S13†). The adsorption capacity of CFF increased from 37.3 to 67.3 mg g^{-1} when the initial As(III) concentration increased from 3.7 to 6.7 mg L^{-1}, implying adsorptive saturation at high aqueous As(III) concentrations. With the increasing initial concentration of As(III), this would produce higher impetus for As(III) to move from the liquid phase to CFF, resulting in more collisions between As(III) and active sites on CFF. However, when the initial concentration of As(III) increased, the removal rate was reduced by nearly half (Table S7†). Obviously, the result indicated that the pH, temperature and initial As(III) concentration profoundly affect the removal efficiency and rate.

3.4. Removal of arsenic in smelting wastewater

The removal of arsenic from the acid effluent was also tested at neutral pH under the aerobic conditions. Although the removal rate of CFF was reduced, the removal efficiency could reach 100%. And the content of arsenic in the aqueous solution during the removal process was determined by ICP-AES

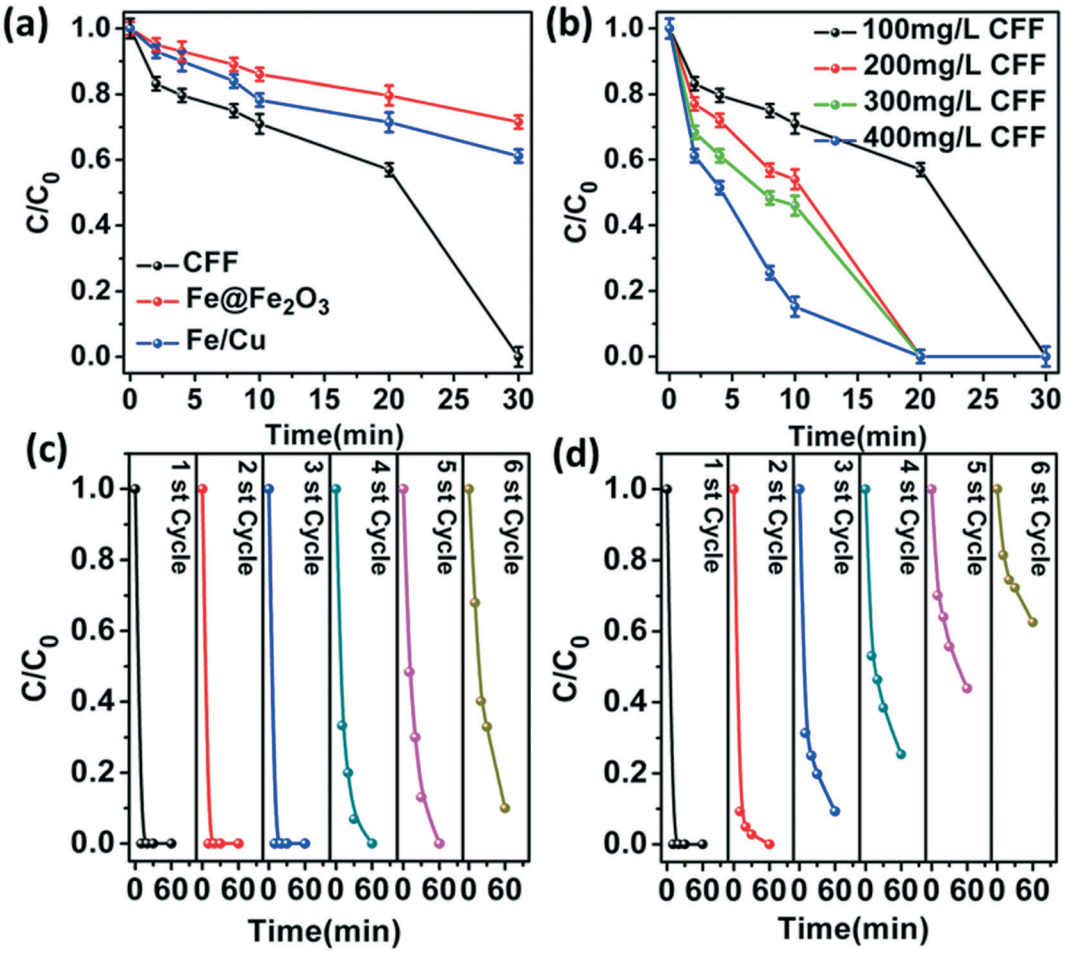

Fig. 7 (a) Removal of total arsenic from smelting wastewater using CFF, Fe/Cu and Fe@Fe_2O_3 under aerobic conditions. (b) Aerobic removal of total arsenic using CFF with different concentrations. Aerobic removal of total arsenic using (c) CFF and (d) nZVI from smelting wastewater after different cycles.

(Table S6†). The results demonstrated that the arsenic content in the treated wastewater has reached the discharge standard (WHO 10 μg L^{-1}). However, the removal efficiencies of the Fe/Cu bimetallic and Fe@Fe_2O_3 catalysts only remained at 40% and 30%, respectively (Fig. 7a). Meanwhile, it shows that the rapid and complete removal of As(III) from the real wastewater samples needed a higher dosing amount of CFF compared with the simulated wastewater (Fig. 7b), possibly owing to the presence of dissolved sulfate and phosphate in the actual wastewater samples (*e.g.*, SO_4^{2-} and PO_3^{2-}) (Table S1†).[16] To further verify the stability of CFF in practical applications, we also carried out stability experiments. The total arsenic removal efficiency by CFF still remained at 90% after 6 consecutive treatments while the removal capacity of nZVI was gradually quenched (Fig. 7c and d). These results indicate that CFF could be an alternative to nZVI for rapidly and efficiently removing arsenic in wastewater.

4. Conclusions

This work fabricated a novel composite material, CFF, through a simple two-step reduction method based on ubiquitous iron and iron oxide. As an adsorbent, CFF provides not only high adsorption capacity and rapid removal rate, but also strong oxidation ability for As(III), thanks to its unique core–shell structure doped with Cu. We demonstrated that doping with Cu could increase the oxygen reduction pathway consisting of a sequential single-electron pathway and a two-electron pathway, which could significantly promote the corrosion of CFF and improve molecular oxygen activation and ROSs production. Meanwhile, environmental researchers previously ascribed the low production of ROSs with nZVI to iron precipitation, high surface reactivity of nZVI toward H_2O_2, and low rates of the Fenton reaction, but usually ignored the significance of the oxygen reduction pathway on molecular oxygen activation and ROS generation, which is unfavorable to the wide application of nZVI. This work suggests that using CFF as adsorbents is a promising strategy to increase the yield of ROSs by adding the oxygen reduction pathway of nZVI. The successful removal of arsenic in smelting wastewater by CFF provides a potential method to reduce the effect of arsenic pollution in the surrounding environment.

Conflicts of interest

There are no conflicts to declare.

Acknowledgements

The study was financially supported by Projects 51579096, 51521006, 51222805 supported by the National Natural Science Foundation of China, the Key Research and Development Program of Hunan Province of China (2017SK2241), and the National Program for Support of Top–Notch Young Professionals of China (2012).

References

1 Y. Zhou, L. Tang, G. Zeng, C. Zhang, Y. Zhang and X. Xie, Current progress in biosensors for heavy metal ions based on DNAzymes/DNA molecules functionalized nanostructures: A review, *Sens. Actuators, B*, 2016, **223**, 280–294.

2 B. Chen, Z. Zhu, S. Liu, J. Hong, J. Ma, Y. Qiu and J. Chen, Facile hydrothermal synthesis of nanostructured hollow iron-cerium alkoxides and their superior arsenic adsorption performance, *ACS Appl. Mater. Interfaces*, 2014, **6**(16), 14016–14025.

3 Z. Cheng, F. Fu, D. D. Dionysiou and B. Tang, Adsorption, oxidation, and reduction behavior of arsenic in the removal of aqueous As(III) by mesoporous Fe/Al bimetallic particles, *Water Res.*, 2016, **96**, 22–31.

4 S. R. Kanel, B. Manning, L. Charlet and H. Choi, Removal of arsenic(III) from groundwater by nanoscale zero-valent iron, *Environ. Sci. Technol.*, 2005, **39**(5), 1291–1298.

5 X. Zhang, M. Wu, H. Dong, H. Li and B. C. Pan, Simultaneous Oxidation and Sequestration of As(III) from Water by Using Redox Polymer-based Fe(III) oxide Nanocomposite, *Environ. Sci. Technol.*, 2017, **51**(11), 6326.

6 J. Tang, L. Tang, H. Feng, G. Zeng, H. Dong, C. Zhang, B. Huang, Y. Deng, J. Wang and Y. Zhou, pH-dependent degradation of p-nitrophenol by sulfidated nanoscale zerovalent iron under aerobic or anoxic conditions, *J. Hazard. Mater.*, 2016, **320**, 581–590.

7 J. Tang, L. Tang, H. Feng, H. Dong, Y. Zhang, S. Liu and G. Zeng, Research Progress of Aqueous Pollutants Removal by Sulfidated Nanoscale Zero-valent Iron, *Acta Chim. Sin.*, 2017, **75**(6), 575.

8 S. R. Kanel, B. Manning, L. Charlet and H. Choi, Removal of arsenic(III) from groundwater by nanoscale zero-valent iron, *Environ. Sci. Technol.*, 2005, **39**(5), 1291–1298.

9 V. Tanboonchuy, N. Grisdanurak and C. H. Liao, Background species effect on aqueous arsenic removal by nano zero-valent iron using fractional factorial design, *J. Hazard. Mater.*, 2012, **205–206**, 40–46.

10 H. Wang, Y. Wu, T. Xiao, X. Yuan, G. Zeng, W. Tu, S. Wu, H. Y. Lee, Y. Z. Tan and J. W. Chew, Formation of quasi-core-shell In_2S_3/anatase TiO_2@metallic $Ti_3C_2T_x$ hybrids with favorable charge transfer channels for excellent visible-light-photocatalytic performance, *Appl. Catal., B*, 2018, **233**, 213–225.

11 H. Wang, Y. Wu, X. Yuan, G. Zeng, J. Zhou, X. Wang and W. C. Jia, Clay-Inspired MXene-Based Electrochemical Devices and Photo-Electrocatalyst: State-of-the-Art Progresses and Challenges, *Adv. Mater.*, 2018, **30**(12), 1704561.

12 H. Wang, X. Yuan, Y. Wu, G. Zeng, W. Tu, C. Sheng, Y. Deng, F. Chen and W. C. Jia, Plasmonic Bi nanoparticles and BiOCl sheets as cocatalyst deposited on perovskite-type $ZnSn(OH)_6$ microparticle with facet-oriented polyhedron for improved visible-light-driven photocatalysis, *Appl. Catal., B*, 2017, **209**, 543–553.

13 M. A. V. Ramos, W. Yan, X. Li, B. E. Koel and W. Zhang, Simultaneous Oxidation and Reduction of Arsenic by Zero-

Valent Iron Nanoparticles: Understanding the Significance of the Core–Shell Structure, *J. Phys. Chem. C*, 2009, **113**(33), 14591–14594.

14 J. Jin, S. Y. Pang and J. Ma, Comment on "Factors Affecting the Yield of Oxidants from the Reaction of Nanoparticulate Zero-Valent Iron and Oxygen", *Environ. Sci. Technol.*, 2008, **42**(4), 1262–1267.

15 Z. Ai, Z. Gao, L. Zhang, W. He and J. J. Yin, Core–Shell Structure Dependent Reactivity of $Fe@Fe_2O_3$ Nanowires on Aerobic Degradation of 4-Chlorophenol, *Environ. Sci. Technol.*, 2013, **47**(10), 5344–5352.

16 L. Tang, H. Feng, T. Jing, G. Zeng, Y. Deng, J. Wang, Y. Liu and Y. Zhou, Treatment of arsenic in acid wastewater and river sediment by $Fe@Fe_2O_3$ nanobunches: The effect of environmental conditions and reaction mechanism, *Water Res.*, 2017, **117**, 175.

17 B. Lai, Y. Zhang, Z. Chen, P. Yang, Y. Zhou and J. Wang, Removal of p-nitrophenol (PNP) in aqueous solution by the micron-scale iron–copper (Fe/Cu) bimetallic particles, *Appl. Catal., B*, 2014, **144**(1), 816–830.

18 S. J. Bransfield, D. M. Cwiertny, K. Livi and D. H. Fairbrother, Influence of transition metal additives and temperature on the rate of organohalide reduction by granular iron: Implications for reaction mechanisms, *Appl. Catal., B*, 2007, **76**(3–4), 348–356.

19 S. J. Bransfield, D. M. Cwiertny, A. L. Roberts and D. H. Fairbrother, Influence of copper loading and surface coverage on the reactivity of granular iron toward 1,1,1-trichloroethane, *Environ. Sci. Technol.*, 2006, **40**(5), 1485–1490.

20 M. Dukkanci, G. Gunduz, S. Yilmaz, Y. C. Yaman, R. V. P. Ko and I. V. Stolyarova, Characterization and catalytic activity of CuFeZSM-5 catalysts for oxidative degradation of Rhodamine 6G in aqueous solutions, *Appl. Catal., B*, 2010, **95**, 270–278.

21 M. Xia, M. Long, Y. Yang, C. Chen, W. Cai and B. Zhou, A highly active bimetallic oxides catalyst supported on Al-containing MCM-41 for Fenton oxidation of phenol solution, *Appl. Catal., B*, 2011, **110**(41), 118–125.

22 M. Danish, X. Gu, S. Lu, A. Ahmad, M. Naqvi, U. Farooq, X. Zhang, X. Fu, Z. Miao and Y. Xue, Efficient transformation of trichloroethylene activated through sodium percarbonate using heterogeneous zeolite supported nano zero valent iron-copper bimetallic composite, *Chem. Eng. J.*, 2017, **308**, 396–407.

23 J. Tang, L. Tang, H. Feng, G. Zeng, H. Dong, C. Zhang, B. Huang, Y. Deng, J. Wang and Y. Zhou, pH-dependent degradation of p-nitrophenol by sulfidated nanoscale zerovalent iron under aerobic or anoxic conditions, *J. Hazard. Mater.*, 2016, **320**, 581–590.

24 Y. Zhou, L. Tang, G. Yang, G. Zeng, Y. Deng, B. Huang, Y. Cai, J. Tang, J. Wang and Y. Wu, Phosphorus–Doped Ordered Mesoporous Carbons embedded with Pd/Fe Bimetal Nanoparticles for the dechlorination of 2,4–dichlorophenol, *Catal. Sci. Technol.*, 2016, **6**(6), 1930–1939.

25 G. Yang, L. Tang, X. Lei, G. Zeng, Y. Cai, X. Wei, Y. Zhou, S. Li, Y. Fang and Y. Zhang, Cd(II) removal from aqueous solution by adsorption on α-ketoglutaric acid-modified magnetic chitosan, *Appl. Surf. Sci.*, 2014, **292**, 710–716.

26 Y. Liu, G. Zeng, L. Tang, Y. Cai, Y. Pang, Y. Zhang, G. Yang, Y. Zhou, X. He and Y. He, Highly effective adsorption of cationic and anionic dyes on magnetic Fe/Ni nanoparticles doped bimodal mesoporous carbon, *J. Colloid Interface Sci.*, 2015, **448**, 451–459.

27 S. R. Kanel, J.-M. Greneche and H. Choi, Arsenic (V) removal from groundwater using nano scale zero-valent iron as a colloidal reactive barrier material, *Environ. Sci. Technol.*, 2006, **40**(6), 2045–2050.

28 C. Noubactep, A critical review on the process of contaminant removal in Fe^0–H_2O systems, *Environ. Technol.*, 2008, **29**(8), 909–920.

29 M. Pagano, A. Volpe, A. Lopez, G. Mascolo and R. Ciannarella, Degradation of chlorobenzene by Fenton-like processes using zero-valent iron in the presence of Feand Cu, *Environ. Technol.*, 2011, **32**(1–2), 155–165.

30 K. Choi and W. Lee, Enhanced degradation of trichloroethylene in nano-scale zero-valent iron Fenton system with Cu(II), *J. Hazard. Mater.*, 2003, **99**(2), 146–153.

31 Z. Xiong, B. Lai, P. Yang, Y. Zhou, J. Wang and S. Fang, Comparative study on the reactivity of Fe/Cu bimetallic particles and zero valent iron (ZVI) under different conditions of N_2, air or without aeration, *J. Hazard. Mater.*, 2015, **297**, 261–268.

32 Y. Du, H. Fan, L. Wang, J. Wang, J. Wu and H. Dai, α-Fe_2O_3 nanowires deposited diatomite: highly efficient absorbents for the removal of arsenic, *J. Mater. Chem. A*, 2013, **1**(26), 7729–7737.

33 H. H. Hassan, E. Abdelghani and M. A. Amin, Inhibition of mild steel corrosion in hydrochloric acid solution by triazole derivatives Part I. Polarization and EIS studies, *Electrochim. Acta*, 2007, **52**(22), 6359–6366.

34 M. J. Alowitz and M. M. Scherer, Kinetics of nitrate, nitrite, and Cr(VI) reduction by iron metal, *Environ. Sci. Technol.*, 2002, **36**(3), 299–306.

35 S. Pang, J. Jiang and J. Ma, Oxidation of Sulfoxides and Arsenic(III) in Corrosion of Nanoscale Zero Valent Iron by Oxygen: Evidence against Ferryl Ions (Fe(IV) as Active Intermediates in Fenton Reaction), *Environ. Sci. Technol.*, 2011, **45**(1), 307–312.

36 G. Dong, Z. Ai and L. Zhang, Total aerobic destruction of azo contaminants with nanoscale zero-valent copper at neutral pH: promotion effect of in-situ generated carbon center radicals, *Water Res.*, 2014, **66**, 22–30.

37 S. S. Hoschek, P. M. Carrica and L. J. Weber, Bubble entrainment and distribution in a model spillway with application to total dissolved gas minimization, *J. Hydraul. Eng.*, 2008, **134**(6), 763–771.

38 M. S. Politano and P. M. Carrica, CagriTuran; L. W., A multidimensional two-phase flow model for the total dissolved gas downstream of spillways, *J. Hydraul. Res.*, 2007, **45**(2), 165–177.

39 H. Zhou, Y. He, Y. Lan, J. Mao and S. Chen, Influence of complex reagents on removal of chromium(VI) by zero-valent iron, *Chemosphere*, 2008, **72**(6), 870–874.

40 N. Oturan, M. Zhou and M. A. Oturan, Metomyl Degradation by Electro-Fenton and Electro-Fenton-Like Processes: A Kinetics Study of the Effect of the Nature and Concentration of Some Transition Metal Ions As Catalyst, *J. Phys. Chem. A*, 2010, **114**(39), 10605–10611.

41 J. I. Nietojuarez, K. Pierzchła, A. Sienkiewicz and T. Kohn, Inactivation of MS_2 coliphage in Fenton and Fenton-like systems: role of transition metals, hydrogen peroxide and sunlight, *Environ. Sci. Technol.*, 2010, **44**(9), 3351–3356.

42 T. T. Nguyen, H. J. Park, J. Y. Kim, H. E. Kim, H. Lee, J. Yoon and C. Lee, Microbial inactivation by cupric ion in combination with H_2O_2: role of reactive oxidants, *Environ. Sci. Technol.*, 2013, **47**(23), 13661–13667.

43 C. Harford and B. Sarkar, ChemInform Abstract: Amino Terminal Cu(II)- and Ni(II)-Binding (ATCUN) Motif of Proteins and Peptides: Metal Binding, DNA Cleavage, and Other Properties, *ChemInform*, 1997, **30**(3), 123–130.

44 Y. Deng, L. Tang, G. Zeng, Z. Zhu, M. Yan, Y. Zhou, J. Wang, Y. Liu and J. Wang, Insight into highly efficient simultaneous photocatalytic removal of Cr(VI) and 2,4-diclorophenol under visible light irradiation by phosphorus doped porous ultrathin g-C_3N_4 nanosheets from aqueous media: Performance and reaction mechanism, *Appl. Catal., B*, 2017, **203**, 343–354.

45 Y. Deng, L. Tang, G. Zeng, C. Feng, H. Dong, J. Wang, H. Feng, Y. Liu, Y. Zhou and Y. Pang, Plasmonic resonance excited dual Z-scheme $BiVO_4$/Ag/Cu_2O nanocomposite: synthesis and mechanism for enhanced photocatalytic performance in recalcitrant antibiotic degradation, Environ. Sci, *NANO*, 2017, **4**(7), 1494–1511.

46 X. Han, J. Song, Y. L. Li, S. Y. Jia, W. H. Wang, F. G. Huang and S. H. Wu, As(III) removal and speciation of Fe (Oxyhydr) oxides during simultaneous oxidation of As(III) and Fe(II), *Chemosphere*, 2016, **147**, 337–344.

47 G. Dong, Z. Ai and L. Zhang, Total aerobic destruction of azo contaminants with nanoscale zero-valent copper at neutral pH: Promotion effect of in-situ generated carbon center radicals, *Water Res.*, 2014, **66**, 22–30.

48 G. Zhang, F. Liu, H. Liu, J. Qu and R. Liu, Respective Role of Fe and Mn Oxide Contents for Arsenic Sorption in Iron and Manganese Binary Oxide: An X-ray Absorption Spectroscopy Investigation, *Environ. Sci. Technol.*, 2014, **48**(17), 10316–10322.

49 C. H. Liu, Y. H. Chuang, T. Y. Chen, Y. Tian, H. Li, M. K. Wang and W. Zhang, Mechanism of Arsenic Adsorption on Magnetite Nanoparticles from Water: Thermodynamic and Spectroscopic Studies, *Environ. Sci. Technol.*, 2015, **49**(13), 7726–7734.

50 C. Wang, H. Luo, Z. Zhang, Y. Wu, J. Zhang and S. Chen, Removal of As(III) and As(V) from aqueous solutions using nanoscale zero valent iron-reduced graphite oxide modified composites, *J. Hazard. Mater.*, 2014, **268**(3), 124–131.

51 H. Zhu, Y. Jia, X. Wu and H. Wang, Removal of arsenic from water by supported nano zero-valent iron on activated carbon, *J. Hazard. Mater.*, 2009, **172**(2–3), 1591–1596.

52 L. Tang, H. Feng, J. Tang, G. Zeng, Y. Deng, J. Wang, Y. Liu and Y. Zhou, Treatment of arsenic in acid wastewater and river sediment by Fe@Fe_2O_3 nanobunches: The effect of environmental conditions and reaction mechanism, *Water Res.*, 2017, **117**, 175–186.

53 G. Zhang, Z. Ren, X. Zhang and J. Chen, Nanostructured iron(III)-copper(II) binary oxide: a novel adsorbent for enhanced arsenic removal from aqueous solutions, *Water Res.*, 2013, **47**(12), 4022–4031.

54 P. Suresh Kumar, R. Q. Flores, C. Sjostedt and L. Onnby, Arsenic adsorption by iron-aluminium hydroxide coated onto macroporous supports: Insights from X-ray absorption spectroscopy and comparison with granular ferric hydroxides, *J. Hazard. Mater.*, 2016, **302**, 166–174.